VI International Conference on Computational Methods for Coupled Problems in Science and Engineering
COUPLED PROBLEMS 2015
B. Schrefler, E. Oñate and M. Papadrakakis (Eds)

COUPLED NUMERICAL MULTIPHYSICS SIMULATION METHODS IN INDUCTION SURFACE HARDENING

DIRK SCHLESSELMANN*, BERNARD NACKE*, ALEXANDER NIKANOROV* AND SERGEY GALUNIN†

* Institute of Electrotechnology (ETP)
Leibniz Universität Hannover
Wilhelm-Busch-Str. 4, D-30167 Hannover, Germany
e-mail: etp@etp.uni-hannover.de, www.etp.uni-hannover.de

† Department of Electrotechnology and Converter Engineering
Electrotechnical State University St. Petersburg
Prof. Popov Str. 5, 197376 St. Petersburg, Russia
email: sagalunin@gmail.com

Key words: Induction Surface Hardening, Induction Heating, Numerical Simulation, Coupled Problems, Multiphysics Problems

Abstract. Numerical simulation is a valuable tool to help investigate complex multiphysics problems of engineering and science. This also applies to inductive surface hardening with its coupled electromagnetic and temperature fields as well as the microstructure changes of the hardened material. In this field, numerical simulation is a well-established approach for effective process design. This is particularly true since an analytical approach usually fails because of the complexity of the problems. Also, experiments oftentimes are not leading to a solution in an acceptable period of time because of the big number of process parameters. Furthermore, numerical simulation can help to investigate effects that could not have been observed otherwise. An example is the Joule heat distribution within a heated work piece during inductive heating. However, the fields of application as well as the methods of numerical simulation have to keep pace with technological progress. Two examples of new applications and methods for numerical simulation in induction hardening are presented in this paper: A complex 3D model of a large bearing and a new approach for the numerical simulation of the martensite microstructure.

1 INTRODUCTION

In the first part of this paper, an application-oriented strategy to numerically model and investigate scan hardening processes for large bearings is introduced. It will be shown how the 3D model can be applied to different hardening setups by a user without deeper knowledge of the numerical software. The advantages of using the model for the development of complex inductor geometries compared to an experiment based approach will be pointed out. The model calculates the temperature profile within a work piece, which is shown exemplarily for an inner ring of a main bearing used in wind power systems.

In the second part of the paper, a new numerical model for calculating martensite microstructure in induction surface hardening processes is introduced. It takes into account the heating as well as the quenching process and uses the temperature history of a work piece to calculate martensite formation. The calculation is based on an empirical equation found by Koistinen and Marburger. A comparison between the heat distribution within a work piece at the end of the heating process and the distribution of martensite after quenching is performed for different process parameters. Thus, it is determined, in which case the temperature distribution is sufficient to predict the hardened layer and in which case the microstructure has to be calculated to receive accurate results. The model is verified by comparing simulation results with experiments.

2 NUMERICAL 3D MODELLING AND VERIFICATION OF INDUCTION SURFACE HARDENING PROCESSES FOR LARGE BEARINGS

The rapid growth of renewable energy all over the world goes hand in hand with technological progress in this field. This also applies to wind power systems with their constantly increasing size and nominal output power of recently up to 8 MW (Vestas V164-8.0). The main bearings of such systems usually have a diameter of several meters. To prevent the bearings from wearing off, their running surfaces have to be hardened. A valid and often used process for this is inductive scan hardening. The process development requires a big financial effort as well as a lot of time because of the size of the bearings and the complexity of the inductors (Figure 1). Therefore, destructive material testing as well as design adaptions of the inductor have to be minimized. This can be achieved with the help of numerical simulation. A numerical 2D model for hardening of the main bearing of a wind power system can be found in [1]. However, to fully understand and calculate the inductive heating process accurately, a full 3D model is required necessarily.

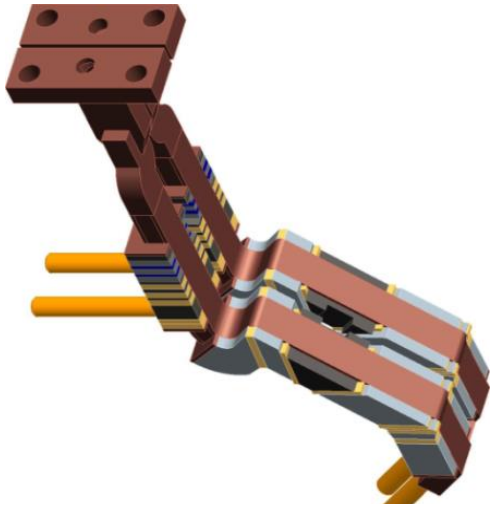

Figure 1: Scanning inductor

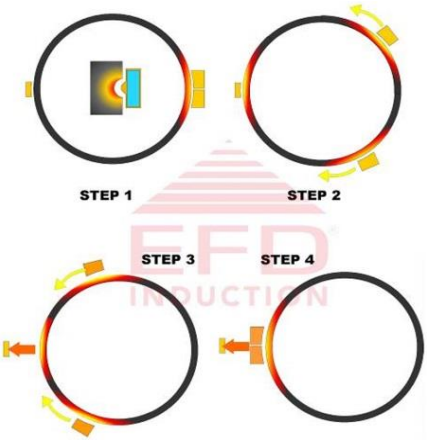

Figure 2: Hardening process

It is crucial for the quality of the hardening process that no soft zones occur. This means an even and seamless hardening profile along the circumference of the bearing is required. To achieve this, the hardening process is divided into four steps which can be seen in Figure 2. In step 1, two scanning inductors remain stationary and heat up the work piece until hardening temperature is reached. After this, for step 2, quenching is initiated and both inductors are moving counter wise along the circumference to harden the work piece simultaneously. With some delay,

depending on the size of the bearing and the feeding speed, a third inductor starts to preheat the zone where the scanning inductors meet again. In step 3, the third inductor is removed right before the scanning inductors reach this final zone. When the scanning process stops the inductors remain motionless and heat up the preheated zone to hardening temperature before they are removed as well. After quenching this area, step 4 and hence the full hardening process is completed [2]. In this paper, only the scanning phase in step 2 will be investigated. It can be regarded as a quasi-stationary process in terms of the temperature profile within the work piece.

2.1 Development of the numerical model

For all calculations the FEM software package ANSYS is used. The algorithm applied to calculate the heating process is shown in Figure 3. Before the calculation starts, the geometry and the mesh are created. Also, a matrix containing the coordinates of all nodes of the work piece is stored. This is required to take into account the relative motion of the inductor. The idea is to move the temperature profile within the work piece along the direction of feeding as explained in [3]. The elements along the direction of movement can be of different size. In order to achieve this, temperatures, usually calculated at each node of an element, are interpolated if necessary.

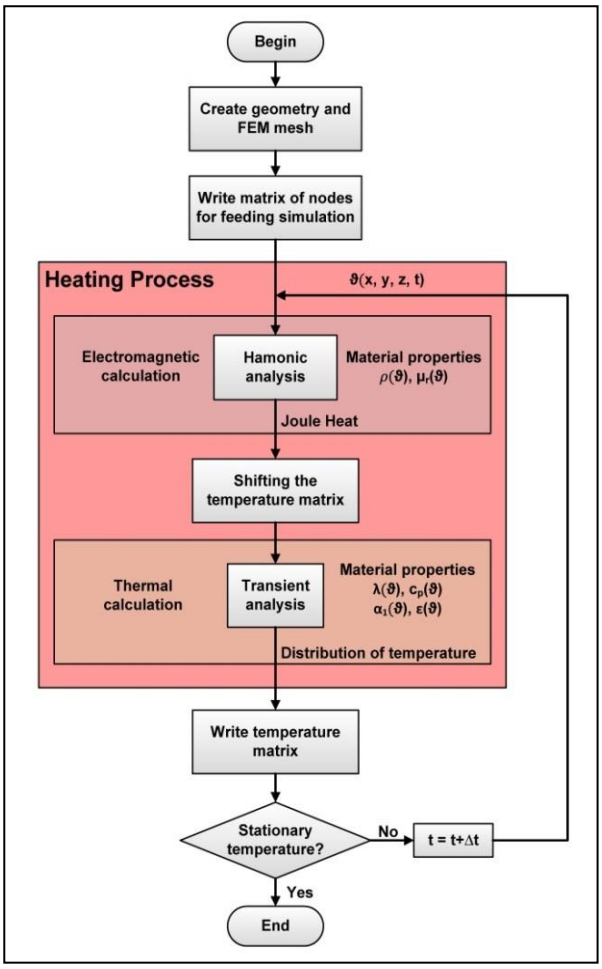

Figure 3: Calculation algorithm

The heating process is divided into sufficiently small time steps and performed as a coupled harmonic-electromagnetic and transient-thermal calculation. The material properties are adjusted after each time step according to the recent temperature within the elements. If a stationary temperature profile is reached, the calculation ends. The result is the quasi-stationary 3D temperature distribution within the work piece. The calculation always starts with the whole system at room temperature. The transient transition period till the stationary state is reached has no relevance and physical significance since the real starting process is not part of the calculation.

The general idea for the 3D model of a complex large scale inductor and bearing is to create the system's geometry based on layers. All layers consist of the same number of geometric points. Their spatial coordinates are stored in simple text files, one for each layer. This way, the user is able to change the geometry by simply editing the text files without

having to use ANSYS. A layer does not have to be plane; the points defining it can differ in all three dimensions. The number of layers is unlimited in principal. The process of building the model from the bottom up at the start of a calculation is automated and does not require any action by the user. The points within each layer are used to define lines and areas. By finally connecting the layers, a 3D volume model is created. However, all geometries investigated have to have the same principal topology, which will be explained further below.

To check if the automated generation of geometry and the calculation are working correctly, a simple setup was implemented and tested (Figure 4). Only the conductors, their field concentrating materials and the work piece are depicted, the surrounding air is suppressed. The setup consists of a flat steel work piece and two current carrying conductors. In this case, the geometry is not varying along the conductors and all points of a layer lie within the same plane. The 11 different layers were created by simply changing the x-coordinate of their points. The amount of volumes between the layers sums up to 81. This topology can only be changed by editing the scripts for the automated creation of geometry. However, almost any setup with two conductors and field concentrators above a work piece can be modelled, which is the typical design approach for scanning inductors of large bearings.

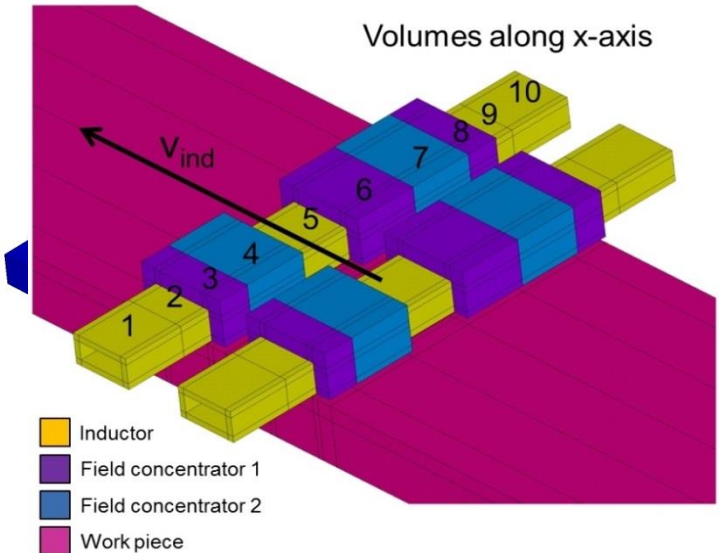

Volume	Field conc. left	Field conc. right	Work piece
1	4	4	4
2	4	4	4
3	2	2	1
4	3	3	1
5	4	4	1
6	2	2	1
7	3	3	1
8	2	2	1
9	4	4	4
10	4	4	4

1 – Work piece
2 – Field concentrator 1
3 – Field concentrator 2
4 – Air (not shown)

Figure 4: Simple test setup

After creating the volumes and the elements of the model, material properties have to be assigned. To keep this procedure as simple as possible, a text file containing the required information is used. The file contains a matrix as shown on the right side of Figure 4: There is a line for each volume along the inductor and four rows. Two rows are used to specify the flux concentrating material of the left and right conductor, one defines if the work piece is present in this layer of volumes. The numbers within the matrix are pointing to the properties of the material in a database. This database can be edited at any time and new materials can be added. The material database and the assignment are completely independent of the geometry. This is a key aspect of the model: It is possible to test different field concentrator variants with the same inductor geometry by only editing the matrix of material parameters.

2.2 Experimental setup

Figure 5: Experimental setup inner ring

The hardening of an inner ring of a large bearing can be seen in Figure 5. A numerical investigation is especially interesting for the inner ring since the design of the inductor is by far more complex compared to the inductor of the outer ring of the bearing. The process used a frequency of 3.8 kHz, the overall system power was about 160 kW. A feeding speed of 5 mm/s was chosen for the inductor. The quenching device is not part of the numerical model since only the temperature distribution within the work piece is analysed in this investigation.

2.3 Verification

The volumetric model of the inductor and the inner ring from the experiment are shown in Figure 6. It consists of the inductor, including all field concentrators, the inner ring and the surrounding air, which again is suppressed in this picture. Additional constructive elements of the inductor are not included in the model since they are irrelevant for the magnetic field distribution. The conductors are not straight, which means that some of the 44 layers that were defined for this model have points in more than one plane. To limit the size of the model, only the volume of the inner ring, which is under influence of the electromagnetic field, is implemented. The curvature of the bearing is relatively small because of its large diameter and is hence neglected. This means that the inner ring in the model is straight with regard to the feeding direction of the inductor. All in all, the model consists of 202,288 elements, which results in a calculation time of some 24 hours till the steady temperature state is reached if a standard PC is used. Thus, a new flux concentrator configuration can be tested within one

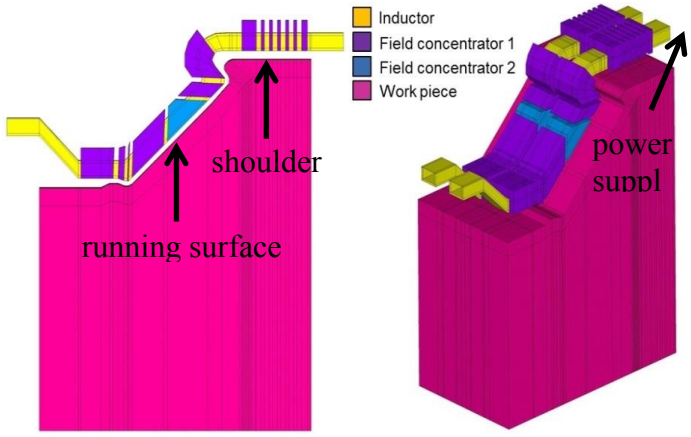

Figure 6: Volumetric model of the experimental setup

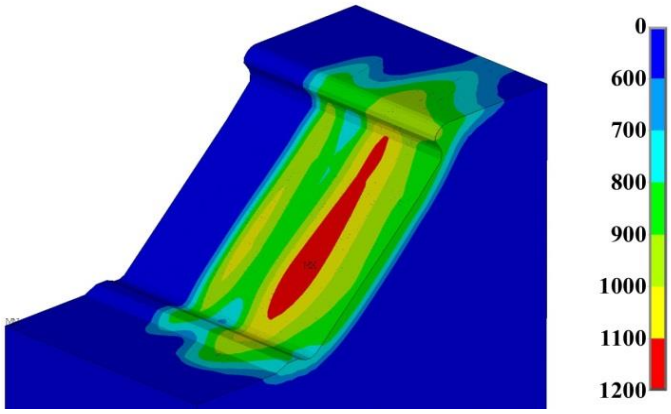

Figure 7: 3D quasi-steady temperature profile

day. For an experiment, field concentrating material would have to be removed and replaced, which is by far more time consuming and expensive.

The model is verified by comparing microsections of a hardened work piece with the quasi-steady temperature profile. The temperature for austenitization is about 850°C in this process and was derived from temperature measurements during experiments. A surface hardening depth (SHD) of about 6 mm is required along the running surface of the inner ring. Usually, the accurate calculation of an SHD of several millimetres has to take into account a calculation of martensite [3]. However, the temperature profile is sufficient to evaluate the hardened zone qualitatively.

Figure 7 shows the quasi-steady temperature profile. The maximum of 1185°C occurs at the edge of the second conductor with regard to the scanning direction where the heated work piece leaves the inductor.

A microsection and a cross-section of the temperature profile are compared in Figure 8. The cross-section is taken from where the maximum temperature occurs. The grey color of the temperature profile shows the area where austenitization was reached. The calculated SHD along the shoulder is smaller in comparison to the microsection. This can be explained by taking a closer look at the gap between inductor and work piece. In this area the gap was 4 mm in the experiment as opposed to 5 mm in the simulation. Furthermore the power connection part of the inductor is not fully implemented in the model. These deviations result in less power being induced in the shoulder area. However, the model is verified with the help of the running surface: Temperature profile and microsection show good agreement since the numerical model is accurate there.

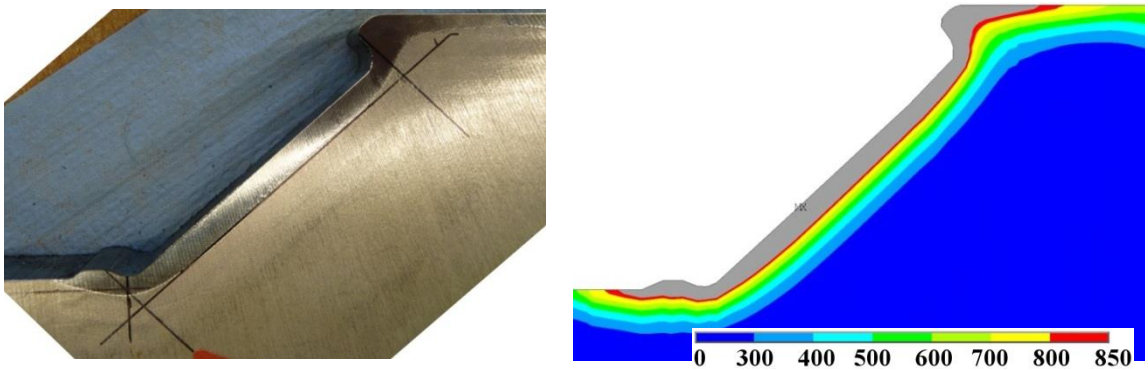

Figure 8: Comparison of microsection and temperature profile

2.4 Conclusions

The model offers an easy way to numerically investigate induction hardening processes of large bearings. The data required for the automated creation of the complex geometry as well as all information about the position and type of flux concentrators is stored in simple text files. This way, no deeper knowledge of the simulation software and calculation algorithm is required to apply the model, given that the topology of the geometry remains unchanged. Results for a new flux concentrator of an existing setup or a modified inductor shape are available within one day. The model was verified by comparing its results to microsections and will be used to effectively develop hardening processes. The costly repetitive process of redesigning the inductor and conducting experiments can be avoided that way.

3 NUMERICAL CALCULATION OF MARTENSITE MICROSTRUCTURE IN INDUCTION SURFACE HARDENING PROCESSES

In the second part of the paper, a new numerical model for calculating martensite microstructure in induction surface hardening processes is introduced. It takes into account the heating as well as the quenching process and uses the temperature history of a work piece to calculate martensite formation. The calculation is based on an empirical equation found by Koistinen and Marburger [4]. Before only coupled electromagnetic and thermal models have been used for the investigation and design of complex induction hardening processes for several years. Instead of calculating martensite formation during quenching, the models have used the temperature distribution at the end of the heating process to predict the microstructure within the work piece [3]. This approach is valid for surface hardening depths which do not exceed a few millimetres. If bigger hardening depths have to be investigated, heat transfer from the surface of the work piece to its core becomes increasingly important. In this case, the temperature distribution might lead to inaccurate predictions of the hardened profile. Furthermore, heat transfer has to be considered, if there is a delay between heating and quenching. This undesirable situation occurs in many industrial hardening processes. To investigate situations as described above, a new algorithm for computing martensite microstructures is applied. The aim is to determine, if there is a critical depth, which requires a martensite calculation. In addition, situations are identified, in which a delay of quenching cannot be neglected. For this, the influence of different quenching situations on the critical depth is investigated.

3.1 Algorithm for calculating martensite microstructures

Subsequent to heating, the quenching process has to be taken into consideration. Therefore, a thermal calculation based on the temperature distribution at the end of the heating process has to be performed. The heat transfer is represented by a coefficient as a function of temperature, which is assigned to all locations on the work piece's surface quenched with cooling agent. Coefficients for different agents and parameters like pressure and flow rate can be found in respective literature [6].

For calculating martensite microstructures the algorithm shown in Figure 9 has to be performed for every node of a FEM model. The algorithm starts with an analysis of each node's temperature

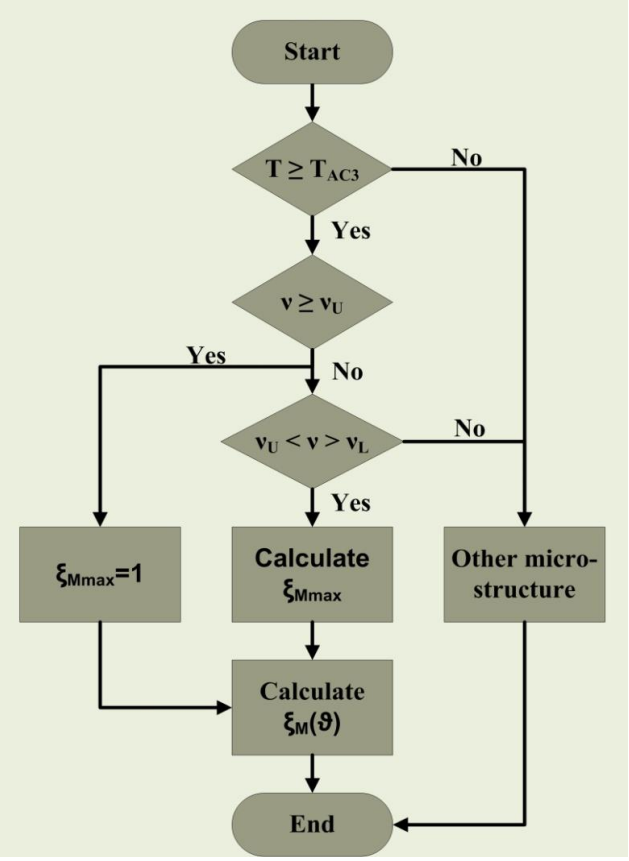

Figure 9: Algorithm for calculating martensite

history. Two conditions have to be met necessarily to receive a fully martensitic microstructure: First, the austenitizing temperature T_{AC3} has to be reached during heating. This is required for a complete austenitic transformation. Secondly, the upper critical cooling rate v_U has to be reached during quenching. Curve 1 in Figure 10 shows a typical time-temperature curve of an inductive hardening process including heating and quenching, which fulfills these conditions. In this case, diffusion of carbon and iron is not possible and microstructures other than martensite cannot form. The fraction of martensite ξ_M can be calculated according to an equation of Wildau and Hougardy [7]:

$$\xi_M(\vartheta) = \left[1 - \exp\left(-c_1(T_{MS} - \vartheta)^{c_2}\right)\right] * 100\% \quad (1)$$

(1) is based on an empirical approach by Koistinen and Marburger [4]. By introducing an additional constant c_2 and taking into account that c_1 and c_2 strongly depend on the material's carbon content, Wildau and Hougardy suggest an equation suitable for a wide range of steels.

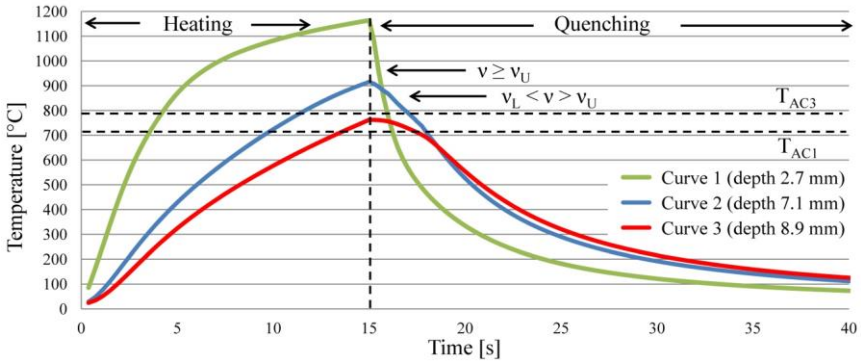

Figure 10: Typical time-temperature curve

The martensite fraction is only a function of the material's temperature ϑ after quenching. The formation of martensite begins below the martensite starting temperature T_{MS}. If the speed of quenching is between v_U and the lower critical cooling rate v_L, diffusion of carbon and iron occurs. Therefore the resulting microstructure contains bainite, ferrite and perlite besides martensite. An example of such time-temperature profiles is given by Curve 2 in Figure 10. (1) has to be extended with a factor ξ_{Mmax}, which represents the maximum martensite fraction at a certain cooling speed v.

$$\xi_M(\vartheta) = \xi_{Mmax}(v) * \left[1 - \exp\left(-c_1(T_{MS} - \vartheta)^{c_2}\right)\right] * 100\% \quad (2)$$

This factor is unity for cooling rates higher than v_U and zero for rates lower than v_L where martensite formation does not occur. To determine ξ_{Mmax}, the contents of bainite ξ_B, ferrite ξ_B and perlite ξ_B are calculated. The residual fraction of martensite is then given by [8]:

$$\xi_{M\_max} = 1 - (\xi_B + \xi_B + \xi_B) \quad (3)$$

Several authors suggest using a semi-empirical approach by Johnson, Mehl and Avrami or Leblond to calculate microstructures occurring in diffusion processes [9-11]. Here, data that is derived from time-temperature transformation (TTT) and continuous cooling transformation (CCT) diagrams or determined by experiments is used to describe the formation. This approach is applied in simulations of many different processes, for example precision forging [12]. However, this paper is focused on calculating the martensite content within a relatively thin layer in induction surface hardening applications. Therefore, a more direct way to determine ξ_{Mmax} is suggested. By using a TTT diagram, ξ_{Mmax} can be determined for different quenching rates. It was found that the relation can be described as:

$$\xi_{Mmax}(v) = 1 - \exp\left[-(v - c_5)/c_6\right] \quad (4)$$

For quenching rates lower then v_U first fractions of martensite occur at lower temperatures T_{MS}. Using data from the same TTT diagram T_{MS} is given as:

$$T_{MS}(v) = -c_3 * \ln(v) + c_4 \quad (5)$$

Both empirical equations are determined by using the method of least squares and show good agreement with data derived from TTT diagrams of various steels. The suggested approach can only be used for quenching processes typical for induction surface hardening. More complex temperature time profiles require the approach of Johnson, Mehl and Avrami or Leblond. Furthermore, the direct approach does not take into consideration that austenite formation already starts at temperatures above T_{AC1} [13]. The calculation only takes into account fully austenitized areas of material.

3.2 Investigation using a basic 1D model

The numerical model used for all basic investigations is one-dimensional and represents the infinite half space. It consists of a current fed inductor 2 mm above a work piece. Carbon steel C45 and alloyed steel 42CrMo4 are investigated exemplarily with their different material parameters [14]. To cover a wide range of hardening depths, frequencies of 62 kHz and 3 kHz are used in the simulation. In addition, a depth d_{TH} (seen from the surface of the work piece) is defined for each simulation. The hardening temperature T_H has to be reached within this depth, meaning that the material is fully austenitized. A constant value T_H, sufficient for the shortest heating time, is assumed to allow better comparability. However, T_H is varied for both frequencies because the initial heating time differs significantly. The parameters for investigating quenching are the delay time t_{delay} between heating and quenching and the intensity $q_{int.}$ of quenching. Water is used for quenching. Quenching is maintained until the maximum temperature within austenitized areas is below 50°C. To be able to compare temperature and martensite distribution, a depth d_M is defined. Within this depth the martensite fraction amounts to 95 % and is therefore considered to be fully martensitic.

Table 1: Investigation with f = 62 kHz and h_{WP} = 100 mm

Material	T_H [°C]	d_{TH} [mm]	d_M [mm]	t_{heat} [s]	t_{delay} [s]	Quenching agent	$q_{int.}$ [m³/s*m²]
C45	925	1,00	1,00	0,27	0	water	2,00
C45	925	2,00	2,00	1,75	0	water	2,00
C45	925	3,00	3,00	6,85	0	water	2,00
42CrMo4	925	3,00	3,00	6,30	0	water	2,00
42CrMo4	925	3,00	3,00	6,30	1,0	water	2,00
42CrMo4	925	3,00	3,00	6,30	0	water	0,28
42CrMo4	925	3,00	3,00	6,30	1,0	water	0,28

Table 1 shows simulation results for a frequency of 62 kHz and a work piece height of 100 mm. The large height of the work piece in relation to the hardening depth of a few millimeters means that the core temperature does not increase during heating. For a value of d_{TH} up to of 3 mm there is no deviation of d_M for C45 as well as 42CrMo4. Larger values of d_{TH} have not been investigated with this frequency because of the small penetration depth. A decrease of

the quenching rate from 2 m³/s*m² to 0.28 m³/s*m² and the influence of a delay of 1 s was checked for 42CrMo4 additionally.

Table 2: Investigation with f = 62 kHz and h_{WP} = 6 mm

Material	T_H [°C]	d_{TH} [mm]	d_M [mm]	t_{heat} [s]	t_{delay} [s]	Quenching agent	$q_{int.}$ [m³/s*m²]
42CrMo4	925	3,00	3,00	2,90	0	water	2,00
42CrMo4	925	3,00	3,00	2,90	0	water	0,28
42CrMo4	925	3,00	3,40	2,90	0,5	water	0,28
42CrMo4	925	3,00	3,72	2,90	0	water	0,28
42CrMo4	925	3,00	4,68	2,90	1,5	water	0,28
42CrMo4	870	3,00	4,44	2,90	1,5	water	2,00

In Table 2 simulation results for a frequency of 62 kHz and a reduced work piece height of 6 mm are shown for 42CrMo4. The austenitization depth d_{TH} has a fixed value of 3 mm, which means that 50 % of the work piece is austenitized after heating. In this case, the heating time of 2.9 is significantly lower than 6.3 s in case of a work piece with a height of 100 mm.

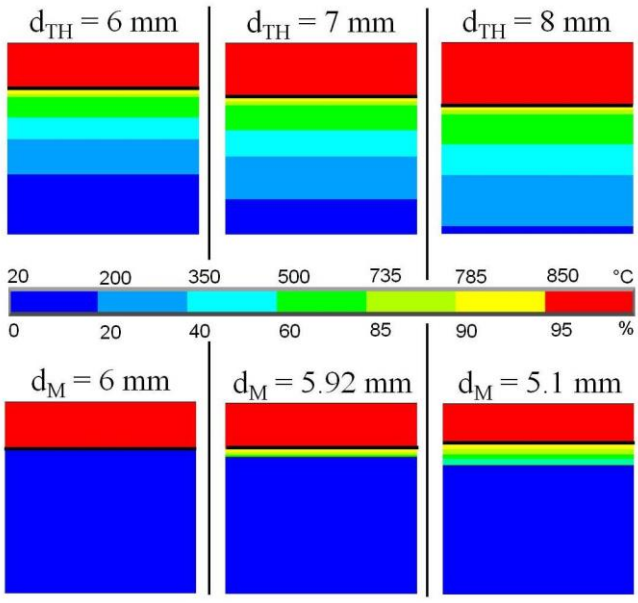

Figure 11: Investigation with f = 3 kHz, h_{WP} = 100 mm and d_{TH} with a value of (a) 6mm, (b) 7 mm and (c) 8 mm

A decrease of the quenching intensity does not affect d_M. A deviation only occurs, if a delay is taken into consideration as well. A delay time of 1.5 s results in 78 % percent of the work piece having a fully martensitic microstructure. If adjusted to the heating time of 2.9 s, T_H has a value of about 870°C. In this case, the deviation decreases and only 74 % of the work piece is fully martensitic. However, the influence of a delay is also evident here. In contrast to a work piece with a height of 100 mm, self-quenching does not occur. The average temperature after heating is much higher. Areas of the work piece further beneath the surface than d_{TH} are austenitized between heating and quenching because the heat cannot be transferred to a cold core.

Table 3: Investigation with f = 3 kHz, h_{WP} = 100 mm and variation of d_{TH}

Material	T_H [°C]	d_{TH} [mm]	d_M [mm]	t_{Heat} [s]	t_{delay} [s]	Quenching agent	$q_{int.}$ [m³/s*m²]
C45	850	6,00	6,00	7,70	0	water	1,20
C45	850	7,00	5,92	11,00	0	water	1,20
C45	850	8,00	5,10	15,00	0	water	1,20

The investigation of hardening with a frequency of 3 kHz is shown in Table 3. The austenitization temperature was defined as 850°C and a quenching intensity of 1.2 m³/s*m² was used. Up to an austenitization depth of 6 mm there is no difference between the temperature and martensite profile. Bigger austenitization depths result in a decrease of the fully martensitic area. This can be also seen in Figure 11, where temperature and martensite profiles are shown for different values d_{TH} from the left to the right. The deviation can be explained by taking a look at the heating times required for achieving these depths. For example, an austenitization depth of 8 mm requires a heating time of 15 s. Temperature curves for this case are illustrated in Figure 10. The amount of heat energy induced into the work piece in that period of time can neither be dissipated fast enough by quenching of the surface with water nor by self-quenching. Therefore, cooling rates are lower than v_U and only fractions of material become martensitic (compare Curve 2 in Figure 10). It can be stated that longer heating times and bigger depths d_{TH} have a negative impact on the depth of full martensite.

3.3 Verification

Figure 12 shows the microsection and simulation results of a hardened straight-cut gear. As described in [5], the gear was heated using simultaneous dual frequency (SDF®) and quenched with a water-air spray cooling afterwards. The temperature profile at the end of the heating process and the microsection show good agreement at the root and the flank of the tooth. However, the microsection shows that the tip of the tooth is almost through hardened, whereas the temperature distribution indicates a hardening profile following the gear's contour. This can be explained by taking a closer look at the assumptions that are made when a temperature distribution is used to predict a hardening profile: As mentioned before,

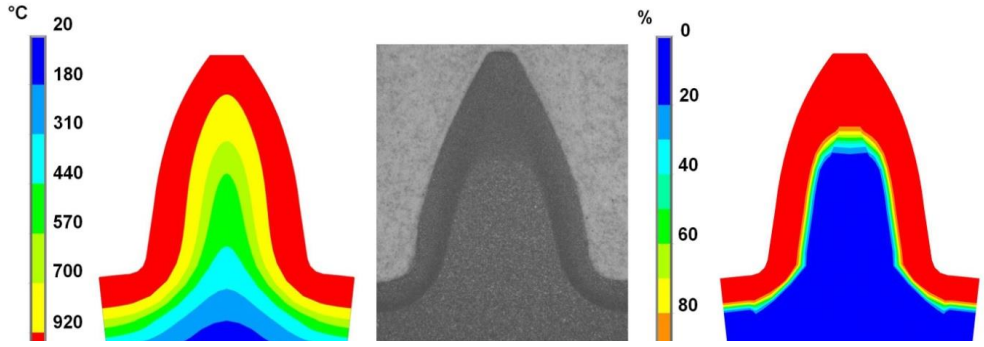

Figure 12: (a) Temperature profile, (b) microsection and (c) martensite profile of a straight cut gear

quenching is supposed to start without any delay after heating. If there is a delay, heat transfer from the surface of the work piece to its core has to be taken into account. The zone of austenitization might increase and therefore the hardened layer might as well. This effect is more pronounced at the tip of a tooth, because heat accumulates in this area, whereas self-quenching occurs in the root area and heat is transferred to the core of the work piece. The actual delay between the end of heating and the start of quenching was 0.4 s in the experiment. If this is considered in the simulation and the new algorithm to compute the martensite microstructure is used, a better agreement of microsection and simulation is evident for the tip: An increased hardening depth as well as the contour being less sharp can be seen if Figure 12 (c) and (a) are compared. The results for root and flank stay unchanged.

3.4 Conclusions

A module for the calculation of quenching and martensite fraction was implemented in the existing simulation tool used for computing inductive surface hardening processes. Investigations with a 1D model have shown that the temperature distribution at the end of the heating process usually is sufficient for a good prediction of the hardened profile if a frequency of several 10's of kHz is used and the height of the work piece is much bigger than the hardening depth. In case of a relatively thin work piece, a delay between heating and quenching as well as the quenching parameters have an influence on the hardening depth and martensite formation has to be calculated to receive accurate results. The verification of the extended simulation tool made evident that a deviation of temperature and martensite profile might also occur when more complex work pieces like gears are hardened with induction. A calculation of martensite should always be performed in such investigations to check, if there is deviation compared to the temperature profile.

REFERENCES

[1] Stiele, H., Brand, M., Asperheim J.-I.: Unterstützung der Prozessentwicklung des induktiven Randschichthärtens großer Lagerringe durch Simulation. Elektrowärme International, Vol. 68, 2010, No. 3, pp. 203-206.
[2] Stiele, H., Schulte, H.: Induction hardening of wind energy plants and components. Heat Processing, Vol. 7, 2009, No. 1, pp. 1-6.
[3] Zedler, T.: Numerische Modellierung, Analyse und Design von induktiven Systemen für das Randschichthärten komplexer Werkstückgeometrien. Sierke-Verlag, Göttingen, 2010, 50 pp.
[4] Koistinen, D. P., Marburger, R. E.: A General Equation Prescribing the Extent of the Austenite-Martensite Transformation in Pure Iron-Carbon Alloys and Plane Carbon Steels. Acta Metallurgica, 7 (1959) p. 59-60.
[5] Schlesselmann, D., Jestremski, M., Rodman, D., Nacke, B.: Numerical Simulation Methods for Complex Induction Hardening Processes. Proceedings of UIE Congress, XVII, St. Petersburg, Russia, (2012) p. 98-103.
[6] Golovin, G., Zamyatin, M.: High frequency heat treatment. Mashinostroenie, Leningrad (1990).
[7] Wildau, M., Hougardy, H.: Zur Auswirkung der Ms-Temperatur auf Spannungen und Maßänderungen. Härterei-Technische Mitteilungen, 42 (1987) p. 261-268.
[8] Börnsen M.: Zum Einfluss von Gefügeumwandlungen auf Spannungen und Formänderung bei thermischer und mechanischer Belastung. VDI-Verlag, Düsseldorf, 1 edition (1989).
[9] Johnson, W. A., Mehl, R. F.: Reaction Kinetics in Process of Nucleation and Growth. Transactions of the AIME, 135 (1939) p. 416-458.
[10] Avrami, M.: Kinetics of Phase Change III. Journal of Chemical Physics, 9 (1941) p. 177-184.
[11] Leblond, J. B., Devaux, J.: A New Kinetic Model for Anisothermal Metallurgical Transformations in Steels Including Effect of Austenite Grain Size. Acta Metallurgica, 32 (1984) p. 137-146.
[12] Behrens, B. A., Bach, F. W., Bouguecha, A., Nürnberger, F., Schaper, M., Yu, Z., Klassen, A.; Numerische Berechnung einer integrierten Wärmebehandlung für präzisionsgeschmiedete Bauteile. Journal of Heat Treatment and Materials, 67 (2012) p. 337-343.
[13] Läpple, V.: Wärmebehandlung des Stahls. Verlag Europa-Lehrmittel, Haan-Gruiten, 10 edition (2010).
[14] Wever, F., Rose, A., Peter, W., Strassburg, W., Rademacher, L.: Atlas zur Wärmebehandlung der Stähle. Verlag Stahleisen, Düsseldorf (1961).